RNA-binding protein Elavl1/HuR is required for maintenance of cranial neural crest specification

Erica J. Hutchins[1], Jose Chacon[2], and Marianne E. Bronner[1]*

[1] Division of Biology & Biological Engineering, California Institute of Technology, Pasadena, CA 91125, USA.
[2] Department of Biology, School of Math and Science, California State University Northridge, Northridge, CA 91330, USA.
*Correspondence: mbronner@caltech.edu

Neural crest development is transcriptionally controlled via sequential activation of gene regulatory networks (GRNs). Recent evidence increasingly implicates a role for post-transcriptional regulation in modulating the output of these regulatory circuits. Using RNA-sequencing data from avian embryos to identify potential post-transcriptional regulators, we observed enrichment during early neural crest development of *Elavl1*, which encodes for the RNA-binding protein HuR. Immunohistochemical analyses revealed expression of HuR following establishment of the neural plate border. Perturbation of HuR resulted in premature neural crest delamination from the neural tube as well as significant reduction in transcripts associated with the neural crest specification GRN (*Axud1* and *FoxD3*), phenotypes also observed with downregulation of the canonical Wnt inhibitor Draxin. RNA pulldown further shows that *Draxin* is a specific target of HuR. Importantly, overexpression of exogenous *Draxin* was able to rescue the cranial neural crest specification defects observed with HuR knockdown. Thus, HuR plays a critical a role in the maintenance of cranial neural crest specification, at least partially via *Draxin* mRNA stabilization. Together, these data highlight an important intersection of post-transcriptional regulation with modulation of the neural crest specification GRN.

INTRODUCTION

Neural crest cells are an essential, multipotent cell population in the vertebrate embryo. During development, these cells must undergo coordinated induction, specification, and epithelial—mesenchymal transition (EMT) events to migrate and ultimately form a myriad of tissues, including craniofacial structures, components of the peripheral nervous system, as well as many other derivatives (Gandhi and Bronner, 2018). The transcriptional control of these events has been dissected and mapped into modules of a feed-forward gene regulatory network (GRN), which help explain the detailed sequence of events involved in neural crest development (Martik and Bronner, 2017; Simoes-Costa and Bronner, 2015; Williams et al., 2019). Recently, there has been growing appreciation for the role that post-transcriptional regulation plays in the establishment, maintenance, and regulation of neural crest formation (Bhattacharya et al., 2018; Sanchez-Vasquez et al., 2019; Ward et al., 2018; Weiner, 2018). However, to date, much of the work on post-transcriptional regulation in neural crest has been focused on the role of microRNAs.

Given that RNA-binding proteins (RBPs) play an essential role in post-transcriptional regulatory processes (Dassi, 2017), we sought to identify RBPs with early roles in neural crest development. To this end, we analyzed available RNA-sequencing datasets (Williams et al., 2019) from specification-stage avian embryos to identify enriched RBP candidates. Using this approach, we identified *Elavl1*, which encodes the RBP HuR, as an enriched transcript in newly formed neural crest cells.

HuR is a nucleocytoplasmic shuttling protein from the ELAV (embryonic lethal abnormal vision) family of RBPs, which have conserved roles in neural development (Ma et al., 1996; Yao et al., 1993). It is a well-established stabilizer of mRNA, a function often mediated via its association with the 3'-untranslated region (3'-UTR) of its mRNA targets (Abdelmohsen and Gorospe, 2010). Interestingly, HuR has been linked to Wnt signaling regulation (Kim et al., 2015; Palomo-Irigoyen et al., 2020), craniofacial development (Katsanou et al., 2009), as well as cancer cell EMT (Wang et al., 2013); as these processes are also associated with neural crest development, we sought to determine the function of HuR in the neural crest.

Here, we describe a role for HuR in specification of cranial neural crest cells. We found that perturbation of HuR led to premature neural crest delamination, as well as significant reduction in the expression of genes regulating the neural crest specification

GRN. We show that these effects were mediated by loss of *Draxin*, a direct mRNA target of HuR. Our data demonstrate a critical role for HuR, and RBP-mediated post-transcriptional control, in the regulation of a critical neural crest specification module.

RESULTS

The RNA-binding protein HuR is expressed in cranial neural crest

Cranial neural crest cells are indispensable for proper craniofacial development (van Limborgh et al., 1983; Vega-Lopez et al., 2018). By analyzing RNA-sequencing datasets from avian embryos at the 5-6 somite (Williams et al., 2019) corresponding to the time at which neural crest specification is complete, we identified enrichment of *Elavl1* transcripts which encodes the RNA-binding protein HuR. Given that HuR knockout mice often display defects in craniofacial structures (Katsanou et al., 2009), we hypothesized a potential role for HuR during cranial neural crest development. To this end, we first examined the expression pattern of HuR in the developing chick embryo. Early in neurulation, when the neural plate border (NPB) is established within the rising neural folds, HuR expression was detected in the anterior open neural tube and closing neural folds surrounding the anterior neuropore but absent from Pax7-expressing NPB cells (**Fig. 1A**). As the neural tube closed, when neural crest specification is complete, HuR expression became enriched throughout the neural tube and overlapped with Pax7 expression in premigratory cranial neural crest cells (**Fig. 1B-C**). Following cranial neural crest epithelial—mesenchymal transition (EMT), HuR remained expressed in the migratory neural crest cells, as well as throughout the brain and neural tube (**Fig. 1D**). Thus, HuR is expressed in specified, premigratory cranial neural crest cells following establishment of the NPB and is retained during the onset of EMT and in early migrating cranial neural crest cells.

HuR downregulation alters cranial neural crest specification and delamination

To determine what, if any, role HuR has in cranial neural crest development, we perturbed HuR function in the early embryo using a translation-blocking antisense morpholino oligo (MO). We co-electroporated a DNA construct driving expression of a fluorescent protein with control or HuR MOs bilaterally into gastrula stage chick embryos, and analyzed neural crest specification using quantitative fluorescent hybridization chain reaction (HCR) to measure neural crest specifier expression at HH9. Given HuR's association with Wnt signaling (Kim et al., 2015) and the essential roles Wnt signaling plays during early neural crest development (Milet and Monsoro-Burq, 2012; Rabadán et al., 2016; Simoes-Costa and Bronner, 2015; Steventon and Mayor, 2012; Wu et al., 2003; Yanfeng et al., 2003), we focused on the Wnt effector *Axud1*, its target and neural crest specifier *FoxD3*, and the Wnt antagonist *Draxin* (Hutchins and Bronner, 2018, 2019; Simoes-Costa et al., 2015). Following HuR knockdown (**Figure 2—Supplement 1**; 61.4 ± 0.9% of the control side, $P < 0.001$, paired *t*-test, n = 5 embryos, 15 sections), we observed significant reduction in the levels of *Axud1* (**Fig. 2A**; 76.9 ± 4.0% of the control side, $P = 0.0295$, paired *t*-test, n = 7 embryos), *FoxD3* (**Fig. 2B**; 61.3 ± 5.5% of the control side, $P = 0.012$, paired *t*-test, n = 10 embryos), and *Draxin* (**Fig. 2C**; 66.5 ± 2.5% of the control side, $P = 0.008$, paired *t*-test, n = 4 embryos) transcripts compared to contralateral control sides (**Fig. 2D**). Thus, HuR knockdown abrogated cranial neural crest specification, as indicated by loss of the early neural crest specifier *FoxD3* and its activator *Axud1*, as well as the EMT regulator *Draxin*.

We also examined Pax7 to assess if HuR knockdown had an effect on maintenance of the NPB. Interestingly, the total number of Pax7+ cells was unaffected with HuR knockdown (101.3 ± 4.5% of the control side, $P = 0.84$, paired *t*-test, n = 4 embryos, 11 sections); however we found significant increase in the number of Pax7+ cells that delaminated from the neural tube (139.4 ± 8.4% of the control side, $P = 0.009$, paired *t*-test), and concomitant decrease in the number of Pax7+ cells retained within the dorsal neural tube (66.0 ± 5.3% of the control side, $P < 0.001$, paired *t*-test) (**Fig. 2E-F**). Taken together, these data suggest that HuR is required during early cranial neural crest development to regulate specification and prevent premature delamination.

Draxin is a HuR target during cranial neural crest specification

We have previously shown that Draxin knockdown induces premature cranial neural crest delamination and loss of neural crest specifier expression (Hutchins and Bronner, 2018), as we observed for HuR knockdown (**Fig. 2**). Given that HuR has been shown to stabilize mRNA targets and that HuR knockdown resulted in loss of *Draxin* (**Fig. 2**), we hypothesized that *Draxin* may be a HuR target during cranial neural crest specification. Consistent with this, we identified several putative HuR binding sites within the Drax-

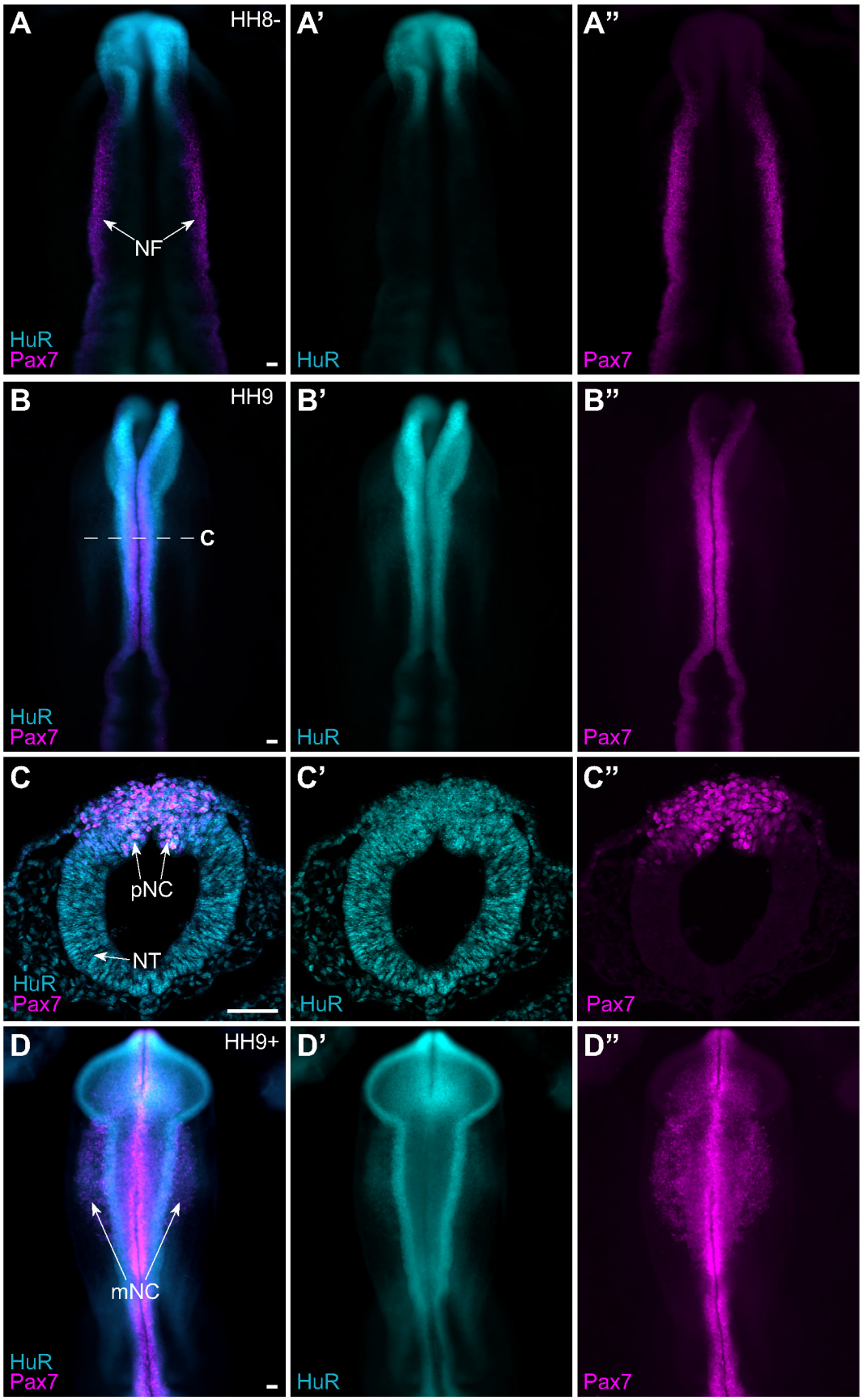

Figure 1. The RNA-binding protein HuR is expressed in cranial neural crest.
(**A-D**) Representative epifluorescence images of wild type HH8- (**A**), HH9 (**B-C**), and HH9+ (**D**) chick embryos, in whole mount (**A**, **B**, **D**) and cross-section (**C**), immunostained for HuR (cyan) and Pax7 (magenta). Dotted white line (**B**) indicates level of cross-section (**C**). NF, neural folds; NT, neural tube; pNC, premigratory neural crest; mNC, migratory neural crest. Scale bar, 50 μm.

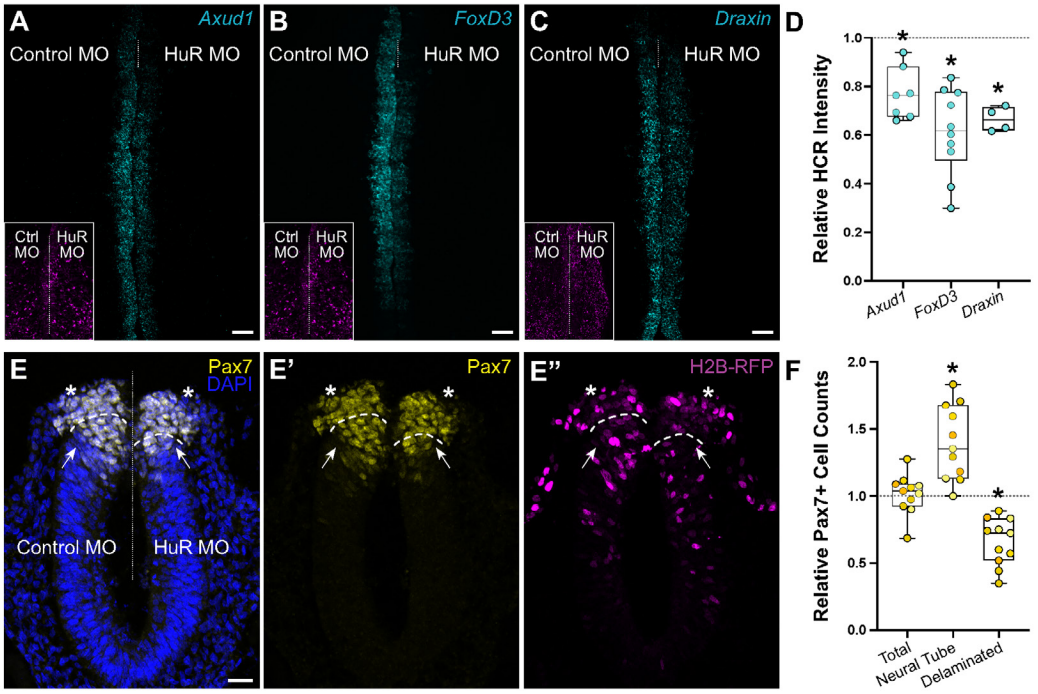

Figure 2. HuR knockdown alters cranial neural crest specification and delamination.
(**A-C**) Representative confocal maximum intensity projection micrographs of HCR processed embryos for *Axud1* (**A**), *FoxD3* (**B**), or *Draxin* (**C**) transcripts in whole mount embryos bilaterally co-electroporated with a fluorescent electroporation control construct (insets) and control morpholino (left) or HuR morpholino (right). Images in (**A**) and (**B**) are from same embryo. Dotted white line indicates midline. Insets show fluorescent electroporation control. MO, morpholino. Scale bar, 50 µm.
(**D**) Relative fluorescence intensity of *Axud1*, *FoxD3*, and *Draxin* for HuR knockdown compared to control sides of individual embryos, calculated as ratio of HuR morpholino versus control morpholino integrated density. *, $P < 0.05$, paired *t*-test.
(**E**) Representative confocal maximum intensity projection micrographs of cross-sectioned embryo bilaterally co-electroporated with a fluorescent electroporation control construct (H2B-RFP) and control morpholino (left) or HuR morpholino (right), immunostained for Pax7 (yellow). Nuclei were stained with DAPI (blue). Dotted white line indicates midline. Dashed white lines indicate limit of dorsal neural tube. Arrows indicate "neural tube" Pax7 cells. Asterisks indicate "delaminated" Pax7 cells. Scale bar, 20 µm.
(**F**) Quantification of the ratio of Pax7+ cells on HuR morpholino (right) versus control morpholino (left) sides of cross-sections. Data are from individual sections; sections from same embryo are displayed in same color (n = 4 embryos, 11 sections) *, $P < 0.01$, paired *t*-test.
See also Figure 2—Supplement 1.

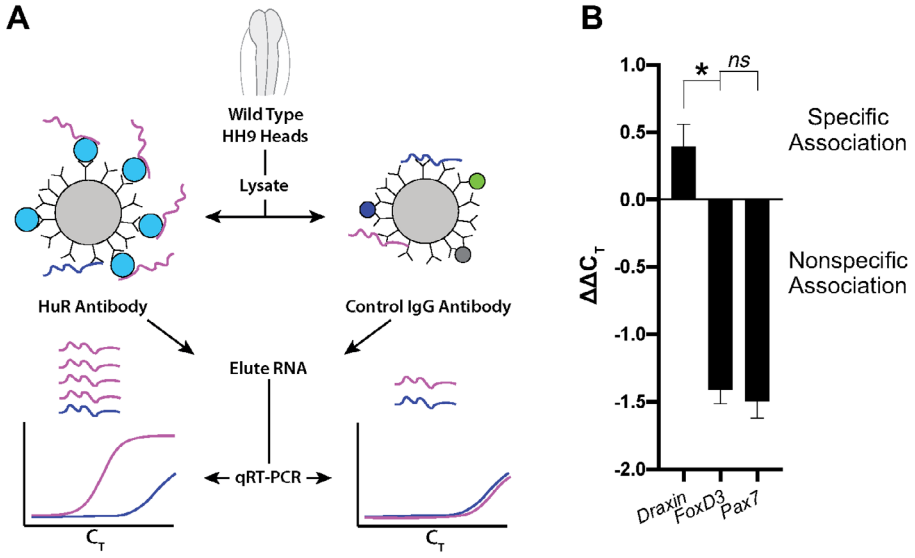

Figure 3. HuR associates with *Draxin* mRNA during cranial neural crest specification.
(**A**) Experimental design of RNA-binding protein/RNA co-immunoprecipitation (RIP) to test RNA association with HuR *in vivo* for neural crest targets. Lysates generated from HH9 heads were incubated with antibody-coated beads for HuR or a non-specific IgG to co-immunoprecipitate protein with bound RNAs. In qRT-PCR, specifically bound RNAs would be more abundant and reach threshold before RNAs that were nonspecific, and therefore would have smaller C_T values. C_T, threshold cycle.
(**B**) Real-time qRT-PCR of RNAs eluted from RIP. ns, non-significant, $P = 0.89$, one-way ANOVA with Tukey's *post hoc* test. *, $P < 0.001$, one-way ANOVA with Tukey's *post hoc* test. $\Delta\Delta C_T$, Average Control IgG ΔC_T − HuR ΔC_T, where ΔC_T = Input C_T − IP C_T. Error bars, SEM.
See also Figure 3—Supplement 1.

in 3'-UTR (**Figure 3—Supplement 1**), To test this possibility, we performed an RNA immunoprecipitation (RIP) followed by quantitative reverse transcription-PCR (qRT-PCR) to pull down endogenous HuR ribonucleoprotein (RNP) complexes. To this end, we incubated lysate generated from wild type HH9 embryonic heads with magnetic beads coated with either HuR antibody or a rabbit IgG non-specific control antibody, then eluted bound RNA and performed qRT-PCR. We expected that RNAs specifically bound by HuR would be significantly enriched compared to non-specifically associated RNAs; this translates to a greater $\Delta\Delta C_T$ value for a target versus a non-target when HuR ΔC_T values (IP fraction normalized to Input) are subtracted from control IgG ΔC_T values (**Fig. 3A**). Given that we observed no change in the total number of Pax7+ cells with HuR knockdown (**Fig. 2**), we classified Pax7 as a non-target, and compared *Draxin* and *FoxD3* $\Delta\Delta C_T$ values to *Pax7* $\Delta\Delta C_T$. We found that *Pax7* and *FoxD3* $\Delta\Delta C_T$ values were negative (i.e. less enriched than the non-specific control IP), and not significantly different from each other ($P = 0.89$, one-way ANOVA with Tukey's post hoc test); however, *Draxin* $\Delta\Delta C_T$ was positive (i.e. enriched over the non-specific control IP), and significantly different from *Pax7* and *FoxD3* $\Delta\Delta C_T$ values ($P < 0.001$, one-way ANOVA with Tukey's post hoc test) (**Fig. 3B**). Thus, these data suggest that *Draxin* is a specific target of HuR, and defects in *FoxD3* may be indirect.

HuR maintains cranial neural crest specification via Draxin mRNA stabilization

Our RIP data suggest that HuR specifically associates with *Draxin* mRNA, but not *FoxD3*. To determine if defects in cranial neural crest specification with HuR knockdown were indirect, we examined

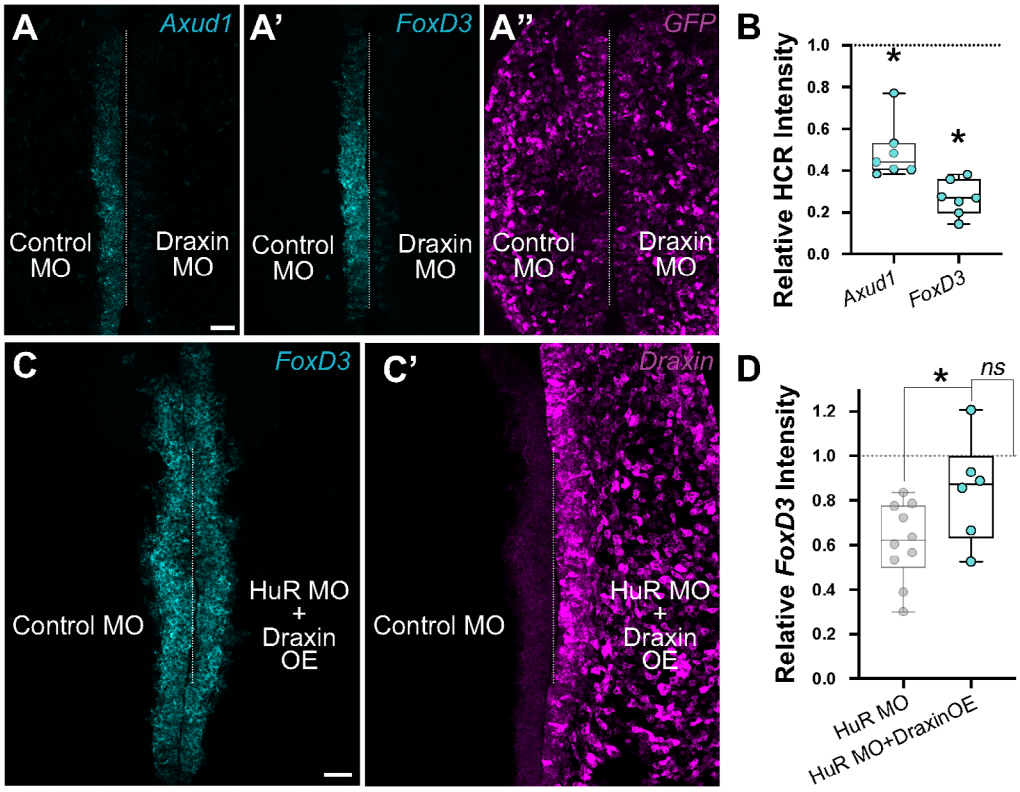

Figure 4. HuR maintains cranial neural crest specification through *Draxin*.

(**A**) Representative confocal maximum intensity projection micrographs of HCR processed embryos for *Axud1* (**A**) or *FoxD3* (**A'**) transcripts in whole mount embryos bilaterally co-electroporated with a fluorescent electroporation control construct (**A''**) and control morpholino (left) or Draxin morpholino (right). Dotted white line indicates midline. MO, morpholino. Scale bar, 50 µm.

(**B**) Relative fluorescence intensity of *Axud1* and *FoxD3* for Draxin knockdown compared to control sides of individual embryos, calculated as ratio of Draxin morpholino versus control morpholino integrated density. *, $P = 0.002$, paired *t*-test.

(**C**) Representative confocal maximum intensity projection micrographs of HCR processed embryo for *FoxD3* (**C**) and *Draxin* (**C'**) transcripts in whole mount embryo bilaterally electroporated with control morpholino (left) or HuR morpholino + Draxin overexpression construct (right). Dotted white line indicates midline. MO, morpholino; OE, overexpression. Scale bar, 50 µm.

(**D**) Relative fluorescence intensity of *FoxD3* for HuR morpholino + Draxin overexpression compared to control sides of individual embryos, calculated as ratio of HuR morpholino + Draxin overexpression versus control morpholino integrated density. HuR morpholino data (gray) were originally presented in Fig. 2 and displayed here for comparison. ns, non-significant, $P = 0.14$, paired t-test. *, $P = 0.02$, unpaired one-tailed *t*-test.

See also Figure 4—Supplement 1.

FoxD3 and *Axud1* expression in Draxin knockdown embryos. As with HuR MO, we electroporated control and Draxin MO (Hutchins and Bronner, 2018, 2019) bilaterally, and performed HCR at HH9. We identified significant reductions in both *Axud1* (48.8 ± 5.1% of the control side, $P = 0.002$, paired *t*-test) and *FoxD3* (26.8 ± 3.2% of the control side, $P < 0.001$, paired *t*-test) with Draxin knockdown (**Fig. 4A-B**). To determine if dysregulation of neural crest specification with HuR knockdown was solely due to loss of *Draxin*, we asked whether *Draxin* upregulation was sufficient to rescue the HuR MO phenotype. To this end, we co-electroporated HuR MO with a *Draxin* overexpression construct (Hutchins and Bronner, 2018, 2019), and assessed neural crest specification with HCR (**Fig. 4C**). Indeed, exogenous *Draxin* was sufficient to significantly restore *FoxD3* expression from HuR knockdown (84.5 ± 9.6% of the control side, $P < 0.02$, unpaired one-tailed *t*-test) to near-control expression levels ($P = 0.14$, paired *t*-test) (**Fig. 4D**).

We also examined the effects of HuR knockdown on cranial neural crest EMT. Consistent with our previous results with Draxin knockdown (Hutchins and Bronner, 2018, 2019), HuR knockdown similarly impeded cranial neural crest emigration (**Figure 4—Supplement 1**; 63.6 ± 4.1% of the control side, $P < 0.001$, paired *t*-test). Given that HuR expression persists during cranial neural crest EMT (**Fig. 1**) when its target *Draxin* is downregulated, HuR may well bind other specific targets necessary for and/or following EMT. Taken together, these data suggest that HuR is required for *Draxin* mRNA stabilization to maintain cranial neural crest specification and likely binds separate targets to facilitate EMT.

DISCUSSION

Our understanding of neural crest development has been greatly increased through the identification of key transcriptional circuits that control its developmental progression. Recent studies suggest a critical role for post-transcriptional regulation in the refinement of the expression outputs of these GRNs. Here, we identified and characterized HuR, an RBP essential for the maintenance of cranial neural crest specification via its regulation of the Wnt antagonist Draxin.

Given that HuR associated endogenously with Draxin mRNA (Fig. 3), and its knockdown resulted in reduced Draxin levels (Fig. 2) and specification defects that were rescued with exogenous expression of the Draxin coding sequence (Fig. 4), we postulate that HuR likely promotes Draxin mRNA stability via interaction with its 3'-UTR. Whereas HuR is known to bind at multiple locations of the transcript for its mRNA targets (Lopez de Silanes et al., 2004), its functions in the enhancement of mRNA stability are largely driven via interaction with AU-rich elements located in 3'-UTRs (Brennan and Steitz, 2001; Lebedeva et al., 2011). Consistent with this hypothesis, using computational analysis (Cook et al., 2011) we identified multiple potential HuR binding sites within the Draxin 3'-UTR (Figure 3—Supplement 1). Further, our Draxin overexpression construct lacked its endogenous 3'-UTR and did not require HuR for stable expression (Fig. 4), unlike the endogenous mRNA, likely accounting for its ability to rescue.

It is important to note that, while HuR expression persists in cranial neural crest during the initiation of EMT and migration, Draxin must be rapidly downregulated for these processes to proceed (Hutchins and Bronner, 2018, 2019). Thus, we hypothesize that HuR becomes endogenously displaced from Draxin at the onset of EMT. RBPs are known to alter association with targets due to post-translational modifications such as phosphorylation or alternative RBP competition (Dassi, 2017; Garcia-Maurino et al., 2017). Indeed, inhibition of serine-threonine kinases has been shown in neural crest to increase cell-cell adhesions and negatively impact cell migration (Monier-Gavelle and Duband, 1995), thus suggesting kinase-driven signaling pathway activation coincident with neural crest EMT. With established roles for serine-threonine phosphorylation in modulating HuR's RNA binding activity and target selection (Grammatikakis et al., 2017), we speculate that HuR phosphorylation at the onset of EMT may facilitate exchange of HuR-bound targets, and promote Draxin release and turnover.

Because its primary target during specification is downregulated while HuR expression persists, this suggests there are likely additional targets and roles for HuR beyond Draxin stabilization. HuR has been shown in other contexts to stabilize Snail1 (Dong et al., 2007) and matrix metalloprotease-9 (MMP-9) (Yuan et al., 2011), factors with well-established roles in neural crest EMT (Cano et al., 2000; Kalev-Altman et al., 2020; Monsonego-Ornan et al., 2012; Strobl-Mazzulla and Bronner, 2012; Taneyhill et al., 2007). Given that the neural crest specification GRN is proceeded by activation of an EMT GRN also coinciding with HuR expression, we speculate that HuR may intersect with additional GRNs following specification.

In summary, we identified a critical role for HuR in the maintenance of cranial neural crest specification. Loss of HuR has deleterious effects on completion

of neural crest specification and delamination due to destabilization of its target, Draxin. The continued expression of HuR during cranial neural crest migration, after Draxin has been endogenously downregulated, suggests additional that HuR may play additional roles at later stages of neural crest development, particularly following EMT and during cell migration.

ACKNOWLEDGMENTS

We thank A. Collazo and G. Spigolon for imaging assistance at the Caltech Biological Imaging Facility; M. Schwarzkopf and G. Shin (Molecular Technologies) for HCR probe design; G. da Silva Pescador and R. Galton for assistance with pilot experiments.

FUNDING

This work was supported by the National Institutes of Health [R01DE027538 and R01DE027568 to M.E.B; K99DE028592 to E.J.H], the Amgen Foundation Caltech Amgen Scholars Program [J.C.], and the California State University—Northridge BUILD PODER program [J.C.].

COMPETING INTERESTS

The authors declare no competing interests.

REFERENCES

Abdelmohsen, K., Gorospe, M., 2010. Posttranscriptional regulation of cancer traits by HuR. Wiley Interdiscip Rev RNA 1, 214-229.

Betancur, P., Bronner-Fraser, M., Sauka-Spengler, T., 2010. Genomic code for Sox10 activation reveals a key regulatory enhancer for cranial neural crest. Proceedings of the National Academy of Sciences of the United States of America 107, 3570-3575.

Bhattacharya, D., Rothstein, M., Azambuja, A.P., Simoes-Costa, M., 2018. Control of neural crest multipotency by Wnt signaling and the Lin28/let-7 axis. Elife 7.

Brennan, C.M., Steitz, J.A., 2001. HuR and mRNA stability. Cell Mol Life Sci 58, 266-277.

Cano, A., Perez-Moreno, M.A., Rodrigo, I., Locascio, A., Blanco, M.J., del Barrio, M.G., Portillo, F., Nieto, M.A., 2000. The transcription factor snail controls epithelial-mesenchymal transitions by repressing E-cadherin expression. Nature cell biology 2, 76-83.

Chacon, J., Rogers, C.D., 2019. Early expression of Tubulin Beta-III in avian cranial neural crest cells. Gene expression patterns : GEP 34, 119067.

Cook, K.B., Kazan, H., Zuberi, K., Morris, Q., Hughes, T.R., 2011. RBPDB: a database of RNA-binding specificities. Nucleic acids research 39, D301-308.

Dassi, E., 2017. Handshakes and Fights: The Regulatory Interplay of RNA-Binding Proteins. Front Mol Biosci 4, 67.

Dong, R., Lu, J.G., Wang, Q., He, X.L., Chu, Y.K., Ma, Q.J., 2007. Stabilization of Snail by HuR in the process of hydrogen peroxide induced cell migration. Biochem Biophys Res Commun 356, 318-321.

Faul, F., Erdfelder, E., Lang, A.G., Buchner, A., 2007. G*Power 3: a flexible statistical power analysis program for the social, behavioral, and biomedical sciences. Behav Res Methods 39, 175-191.

Gandhi, S., Bronner, M.E., 2018. Insights into neural crest development from studies of avian embryos. The International journal of developmental biology 62, 183-194.

Gandhi, S., Hutchins, E.J., Maruszko, K., Park, J.H., Thomson, M., Bronner, M.E., 2020. Bimodal function of chromatin remodeler Hmga1 in neural crest induction and Wnt-dependent emigration. Elife 9.

Garcia-Maurino, S.M., Rivero-Rodriguez, F., Velazquez-Cruz, A., Hernandez-Vellisca, M., Diaz-Quintana, A., De la Rosa, M.A., Diaz-Moreno, I., 2017. RNA Binding Protein Regulation and Cross-Talk in the Control of AU-rich mRNA Fate. Front Mol Biosci 4, 71.

Grammatikakis, I., Abdelmohsen, K., Gorospe, M., 2017. Posttranslational control of HuR function. Wiley Interdiscip Rev RNA 8.

Hamburger, V., Hamilton, H.L., 1951. A series of normal stages in the development of the chick embryo. J Morphol 88, 49-92.

Hutchins, E.J., Bronner, M.E., 2018. Draxin acts as a molecular rheostat of canonical Wnt signaling to control cranial neural crest EMT. The Journal of cell biology 217, 3683-3697.

Hutchins, E.J., Bronner, M.E., 2019. Draxin alters laminin organization during basement membrane remodeling to control cranial neural crest EMT. Developmental biology 446, 151-158.

Hutchins, E.J., Szaro, B.G., 2013. c-Jun N-terminal kinase phosphorylation of heterogeneous nuclear ribonucleoprotein K regulates vertebrate axon outgrowth via a posttranscriptional mechanism. The Journal of neuroscience : the official journal of the Society for Neuroscience 33, 14666-14680.

Jayaseelan, S., Doyle, F., Tenenbaum, S.A., 2014. Profiling post-transcriptionally networked mRNA subsets using RIP-Chip and RIP-Seq. Methods 67, 13-19.

Kalev-Altman, R., Hanael, E., Zelinger, E., Blum, M., Monsonego-Ornan, E., Sela-Donenfeld, D., 2020. Conserved role of matrix metalloproteases 2 and 9 in promoting the migration of neural crest cells in avian and mammalian embryos. FASEB J 34, 5240-5261.

Katsanou, V., Milatos, S., Yiakouvaki, A., Sgantzis, N., Kotsoni, A., Alexiou, M., Harokopos, V., Aidinis, V., Hemberger, M., Kontoyiannis, D.L., 2009. The RNA-binding protein Elavl1/HuR is essential for placental branching morphogenesis and embryonic development. Molecular and cellular biology 29, 2762-2776.

Kim, I., Hur, J., Jeong, S., 2015. HuR represses Wnt/beta-catenin-mediated transcriptional activity by promoting cytoplasmic localization of beta-catenin. Biochem Biophys Res Commun 457, 65-70.

Lebedeva, S., Jens, M., Theil, K., Schwanhausser, B., Selbach, M., Landthaler, M., Rajewsky, N., 2011. Transcriptome-wide analysis of regulatory interactions of the RNA-binding protein HuR. Mol Cell 43, 340-352.

Lopez de Silanes, I., Zhan, M., Lal, A., Yang, X., Gorospe, M., 2004. Identification of a target RNA motif for RNA-binding protein HuR. Proceedings of the National Academy of Sciences of the United States of America 101, 2987-2992.

Ma, W.J., Cheng, S., Campbell, C., Wright, A., Furneaux, H., 1996. Cloning and characterization of HuR, a ubiquitously expressed Elav-like protein. The Journal of biological chemistry 271, 8144-8151.

Manohar, S., Camacho, A., Rogers, C.D., 2020. Cadherin-11 is required for neural crest determination and survival. bioRxiv, 2020.2005.2018.066613.

Martik, M.L., Bronner, M.E., 2017. Regulatory Logic Underlying Diversification of the Neural Crest. Trends Genet.

Megason, S.G., McMahon, A.P., 2002. A mitogen gradient of dorsal midline Wnts organizes growth in the CNS. Development 129, 2087-2098.

Milet, C., Monsoro-Burq, A.H., 2012. Neural crest induction at the neural plate border in vertebrates. Developmental biology 366, 22-33.

Monier-Gavelle, F., Duband, J.L., 1995. Control of N-cadherin-mediated intercellular adhesion in migrating neural crest cells in vitro. J Cell Sci 108 (Pt 12), 3839-3853.

Monsonego-Ornan, E., Kosonovsky, J., Bar, A., Roth, L., Fraggi-Rankis,

V., Simsa, S., Kohl, A., Sela-Donenfeld, D., 2012. Matrix metalloproteinase 9/gelatinase B is required for neural crest cell migration. Developmental biology 364, 162-177.

Palomo-Irigoyen, M., Perez-Andres, E., Iruarrizaga-Lejarreta, M., Barreira-Manrique, A., Tamayo-Caro, M., Vila-Vecilla, L., Moreno-Cugnon, L., Beitia, N., Medrano, D., Fernandez-Ramos, D., Lozano, J.J., Okawa, S., Lavin, J.L., Martin-Martin, N., Sutherland, J.D., de Juan, V.G., Gonzalez-Lopez, M., Macias-Camara, N., Mosen-Ansorena, D., Laraba, L., Hanemann, C.O., Ercolano, E., Parkinson, D.B., Schultz, C.W., Arauzo-Bravo, M.J., Ascension, A.M., Gerovska, D., Iribar, H., Izeta, A., Pytel, P., Krastel, P., Provenzani, A., Seneci, P., Carrasco, R.D., Del Sol, A., Martinez-Chantar, M.L., Barrio, R., Serra, E., Lazaro, C., Flanagan, A.M., Gorospe, M., Ratner, N., Aransay, A.M., Carracedo, A., Varela-Rey, M., Woodhoo, A., 2020. HuR/ELAVL1 drives malignant peripheral nerve sheath tumor growth and metastasis. J Clin Invest 130, 3848-3864.

Rabadán, M.A., Herrera, A., Fanlo, L., Usieto, S., Carmona-Fontaine, C., Barriga, E.H., Mayor, R., Pons, S., Marti, E., 2016. Delamination of neural crest cells requires transient and reversible Wnt inhibition mediated by Dact1/2. Development 143, 2194-2205.

Sanchez-Vasquez, E., Bronner, M.E., Strobl-Mazzulla, P.H., 2019. Epigenetic inactivation of miR-203 as a key step in neural crest epithelial-to-mesenchymal transition. Development 146.

Simoes-Costa, M., Bronner, M.E., 2015. Establishing neural crest identity: a gene regulatory recipe. Development 142, 242-257.

Simoes-Costa, M., Stone, M., Bronner, M.E., 2015. Axud1 Integrates Wnt Signaling and Transcriptional Inputs to Drive Neural Crest Formation. Developmental cell 34, 544-554.

Steventon, B., Mayor, R., 2012. Early neural crest induction requires an initial inhibition of Wnt signals. Developmental biology 365, 196-207.

Strobl-Mazzulla, P.H., Bronner, M.E., 2012. A PHD12-Snail2 repressive complex epigenetically mediates neural crest epithelial-to-mesenchymal transition. The Journal of cell biology 198, 999-1010.

Taneyhill, L.A., Coles, E.G., Bronner-Fraser, M., 2007. Snail2 directly represses cadherin6B during epithelial-to-mesenchymal transitions of the neural crest. Development 134, 1481-1490.

van Limborgh, J., Lieuw Kie Song, S.H., Been, W., 1983. Cleft lip and palate due to deficiency of mesencephalic neural crest cells. Cleft Palate J 20, 251-259.

Vega-Lopez, G.A., Cerrizuela, S., Tribulo, C., Aybar, M.J., 2018. Neurocristopathies: New insights 150 years after the neural crest discovery. Developmental biology.

Wang, J., Guo, Y., Chu, H., Guan, Y., Bi, J., Wang, B., 2013. Multiple functions of the RNA-binding protein HuR in cancer progression, treatment responses and prognosis. Int J Mol Sci 14, 10015-10041.

Ward, N.J., Green, D., Higgins, J., Dalmay, T., Munsterberg, A., Moxon, S., Wheeler, G.N., 2018. microRNAs associated with early neural crest development in Xenopus laevis. BMC Genomics 19, 59.

Weiner, A.M.J., 2018. MicroRNAs and the neural crest: From induction to differentiation. Mechanisms of development 154, 98-106.

Williams, R.M., Candido-Ferreira, I., Repapi, E., Gavriouchkina, D., Senanayake, U., Ling, I.T.C., Telenius, J., Taylor, S., Hughes, J., Sauka-Spengler, T., 2019. Reconstruction of the Global Neural Crest Gene Regulatory Network In Vivo. Developmental cell 51, 255-276 e257.

Wu, J., Saint-Jeannet, J.P., Klein, P.S., 2003. Wnt-frizzled signaling in neural crest formation. Trends Neurosci 26, 40-45.

Yanfeng, W., Saint-Jeannet, J.P., Klein, P.S., 2003. Wnt-frizzled signaling in the induction and differentiation of the neural crest. Bioessays 25, 317-325.

Yao, K.M., Samson, M.L., Reeves, R., White, K., 1993. Gene elav of Drosophila melanogaster: a prototype for neuronal-specific RNA binding protein gene family that is conserved in flies and humans. Journal of neurobiology 24, 723-739.

Yuan, Z., Sanders, A.J., Ye, L., Wang, Y., Jiang, W.G., 2011. Knockdown of human antigen R reduces the growth and invasion of breast cancer cells in vitro and affects expression of cyclin D1 and MMP-9. Oncol Rep 26, 237-245.

Zuker, M., 2003. Mfold web server for nucleic acid folding and hybridization prediction. Nucleic acids research 31, 3406-3415.

METHODS

Model organism and embryo collection

Fertile chicken eggs (Gallus gallus) were purchased locally (Sunstate Ranch, Sylmar, CA), and incubated in a humidified 37ºC incubator to the specified Hamburger-Hamilton (HH) stage (Hamburger and Hamilton, 1951). Live embryos were removed from eggs with Whatman filter paper as described (Hutchins and Bronner, 2018, 2019) and stored in Ringer's solution until further processing.

Immunohistochemistry and Hybridization Chain Reaction

For whole mount immunohistochemistry, embryos were fixed at room temperature for 20 min with 4% paraformaldehyde in sodium phosphate buffer. For cross-sections, embryos were fixed at room temperature for 1 h, then washed, embedded, and cryosectioned as described (Hutchins and Bronner, 2018, 2019) prior to immunohistochemistry. Washes, blocking (10% donkey serum), and antibody incubations were performed in TBSTx (0.5 M Tris-HCl/1.5 M NaCl/10 mM $CaCl_2$/0.5% Triton X-100/0.001% Thimerosal) as described (Chacon and Rogers, 2019; Manohar et al., 2020). Primary antibodies are listed in the Key Resources Table. Species-specific secondary antibodies were labeled with Alexa Fluor 568 and 647 (Invitrogen) and used at 1:1000 or 1:500, respectively. For nuclear staining on cross-sections, DAPI (4',6-Diamidino-2-Phenylindole) was added to the secondary antibody solution at [14.3 µM] final concentration. Coverslips were mounted using Fluoromount-G (SouthernBiotech).

Hybridization Chain Reaction (HCR) was performed as described (Gandhi et al., 2020). Embryos were fixed at room temperature for 1 h with 4% paraformaldehyde in phosphate buffered saline (PBS) prior to HCR processing. Custom HCR probes were designed and ordered through Molecular Technologies.

Gene expression constructs and perturbation

Translation-blocking antisense morpholino oligo for HuR (Gene Tools; Key Resources Table) was designed to span the Elavl1 (NCBI NM_204833.1) start

codon from nucleotide −20 to +5 (HuR MO), and electroporated at [2 mM]. Draxin MO was described previously (Hutchins and Bronner, 2018, 2019), and electroporated at [1 mM]. The standard control MO (Gene Tools) was used for contralateral control electroporation. MOs were co-electroporated with pCIG (Megason and McMahon, 2002) or pCI-H2B-RFP (Betancur et al., 2010) to increase electroporation efficiency and to visualize successfully electroporated cells. The Draxin-FLAG construct to drive overexpression (Draxin OE) and the GFP-tagged stabilized β-catenin (NC1-Δ90βcat) construct were described previously (Hutchins and Bronner, 2018, 2019). Electroporations were performed on HH4 gastrula stage chicken embryos as described previously (Hutchins and Bronner, 2018, 2019).

RNA immunoprecipitation (RIP) and qRT-PCR

RNA immunoprecipitation (RIP) was performed as described (Hutchins and Szaro, 2013; Jayaseelan et al., 2014), with minor modifications. Briefly, Protein-G Dynabeads were washed with NT-2 (50 mM Tris-HCl, 150 mM NaCl, 1 mM $MgCl_2$, 0.05% NP-40), blocked in NT-2/5% BSA for 1 h at room temperature, then incubated with 5 µg antibody (HuR IgG or Control IgG) in NT-2/5% BSA for 1 h at room temperature. Following antibody incubation, antibody-coated beads were washed with NT-2 and resuspended in NET-2 (NT-2, 20 mM EDTA, 400 U RNaseOUT, 1x cOmplete, Mini EDTA-free Protease Inhibitor) until addition of cleared lysate.

Embryonic heads were dissected in Ringer's solution, washed in RNase-free PBS, and dissociated in Accumax (Innovative Cell Technologies) for 15 min at room temperature. Following dissociation, cells were pelleted at 2000 x g for 4 min at 4ºC, washed in RNase-free PBS, and resuspended in Polysome Lysis Buffer (0.1 M KCl, 5 mM $MgCl_2$, 10 mM HEPES, 0.5% NP-40, 200 U RNaseOUT, 1x cOmplete, Mini EDTA-free Protease Inhibitor). Cells were frozen at −80ºC overnight to complete lysis and reduce adventitious binding. Lysate was then thawed on ice, vortexed, and centrifuged at 14,000 x *g* for 10 min at 4ºC to remove cellular debris, then cleared lysate was added to antibody-coated beads in NET-2. Immediately following addition of cleared lysate, 10% was removed to serve as an Input control. IP reaction was tumbled at room temperature for 1 h, beads were then washed in NT-2, and RNA was eluted in Proteinase K Buffer (NT-2, 1% SDS, 1.2 mg/mL Proteinase K) for 30 min at 55ºC and phenol/chloroform extracted.

RNA from Input and IP samples was reverse transcribed using SuperScript III and oligo dT priming. Following reverse transcription, we performed qPCR using FastStart Universal SYBR Green Master (Rox) with cDNA (diluted 1:5) and gene-specific primers (Key Resources Table) on a QuantStudio 3 Real-Time PCR System (Applied Biosystems) in triplicate. We determined ΔC_T (ΔC_T = Input C_T − IP C_T) for Draxin, FoxD3, and Pax7 for HuR and Control IgG RIP samples, then calculated $\Delta\Delta C_T$ values ($\Delta\Delta C_T$ = Average Control IgG ΔC_T − HuR ΔC_T) for each target and replicate.

Image acquisition and analysis

Confocal images were acquired using an upright Zeiss LSM 880 at the Caltech Biological Imaging Facility, and epifluorescence images were acquired using a Zeiss Imager.M2 with an ApoTome.2 module. Images were minimally processed for brightness/contrast and pseudocolored using Fiji (ImageJ, NIH) and Adobe Photoshop 2020.

Relative fluorescence intensity was determined in Fiji. For each whole mount image, the line tool was used to draw an ROI surrounding the area of neural crest indicated by positive HCR fluorescence for the genes examined. For cross-sections, ROIs were drawn surrounding the neural crest and neural tube based on tissue morphology from nuclear staining. Following background subtraction (50-pixel rolling ball radius), integrated density was quantified for the ROIs on the control electroporated (left) and experimental electroporated (right) sides from the same embryo. Relative fluorescence intensity was then calculated by dividing the integrated density measurements for the experimental versus the control side of the same embryo.

Pax7 cell counts were performed as described (Hutchins and Bronner, 2018). The limit of the dorsal neural tube and characterization of cells as "delaminated" or "neural tube" was determined based on tissue morphology from nuclear staining. For relative migration distance determined from Pax7-stained embryos, distance of migration was measured in Fiji as described (Hutchins and Bronner, 2018).

RNA structure and HuR binding site prediction

Secondary structure for the Draxin 3'-UTR (GenBank: AB427147.1) was predicted using 'mfold' web server (Zuker, 2003). HuR binding sites were predicted using RBPDB (Cook et al., 2011).

Statistical analyses

Statistical analyses were performed using Prism

(8; GraphPad Software). *P* values are defined in the text, and significance was established with $P < 0.05$. *P* values were calculated using paired t-tests, one-way ANOVA with *post hoc* Tukey, or unpaired t-tests as indicated in the text; tests were two-tailed unless otherwise specified in the text/legend. Data measuring fluorescence intensities or cell counts for Experimental/Control sides are presented as box plots with individual data points shown. Bar graphs representing qPCR $\Delta\Delta C_T$ are presented as mean values, with error bars indicating SEM. Number of embryos and replicates are indicated in figure legends and/or text. Data were assumed to be normally distributed but were not formally tested. *Post hoc* power analyses (Faul et al., 2007) confirmed sufficient statistical power was reached (≥0.8) for reported *P* values and sample sizes.

KEY RESOURCES TABLE

Reagent or resource	Source	Identifier
Antibodies		
Pax7; Species: Mouse IgG1	Developmental Studies Hybridoma Bank	Cat# pax7, RRID:AB_528428
HuR/Elavl1; Species: Rabbit	Abcam	Cat# ab196626
IgG, polyclonal - Isotype Control (ChIP Grade); Species: Rabbit	Abcam	Cat# ab171870
Chemicals, Peptides, and Recombinant Proteins		
Fluoromount-G	SouthernBiotech	Cat# 0100-01
DAPI	Thermo Fisher	Cat# D1306
FastStart Universal SYBR Green Master (Rox)	Millipore/Sigma	Cat# FSUSGMMRO
SuperScript III Reverse Transcriptase	Thermo Fisher	Cat# 18080044
cOmplete, Mini, EDTA-free Protease Inhibitor	Millipore/Sigma	Cat# 11836170001
RNaseOUT Recombinant Ribonuclease Inhibitor	Thermo Fisher	Cat# 10777019
Accumax	Innovative Cell Technologies, Inc	Cat# AM105
Protein G Dynabeads	Thermo Fisher	Cat# 10003D
Experimental Models: Organisms/Strains		
Gallus gallus	Sun State Ranch (Monrovia, CA, USA)	N/A
Oligonucleotides		
HuR morpholino: GACATCTTATAACGTATCTCGCTGC	This paper; GeneTools	N/A
Control morpholino: CCTCTTACCTCAGTTACAATTTATA	GeneTools	N/A
Draxin morpholino: AAGGTGGAAGAAGCTGCCATAATCC	Hutchins and Bronner, 2018; GeneTools	N/A
Draxin qPCR F Primer: CTACGCTGTTATGCCAAATTCC	This paper; IDT	N/A
Draxin qPCR R Primer: GAATGATCCCTGCTCTCCATT	This paper; IDT	N/A
FoxD3 qPCR F Primer: CATCTGCGAGTTCATCAGCA	This paper; IDT	N/A
FoxD3 qPCR R Primer: TTCACGAAGCAGTCGTTGAG	This paper; IDT	N/A
Pax7 qPCR F Primer: CAAACCAACTCGCAGCATTC	This paper; IDT	N/A
Pax7 qPCR R Primer: CTGCCTCCATCTTGGGAAAT	This paper; IDT	N/A
Recombinant DNA		
pCI-H2B-RFP	Betancur et al., 2010	N/A
pCIG	Megason and McMahon, 2002	N/A
Draxin-FLAG	Hutchins and Bronner, 2018	N/A
Software and Algorithms		
Prism8	GraphPad	N/A
ImageJ64	NIH	N/A
Fiji	Schindelin et al., 2012	N/A
QuantStudio Design & Analysis software, version 2.4	Life Technologies	N/A
Zen 2 Blue	Zeiss	N/A
Zen Black	Zeiss	N/A
Photoshop CC	Adobe	N/A

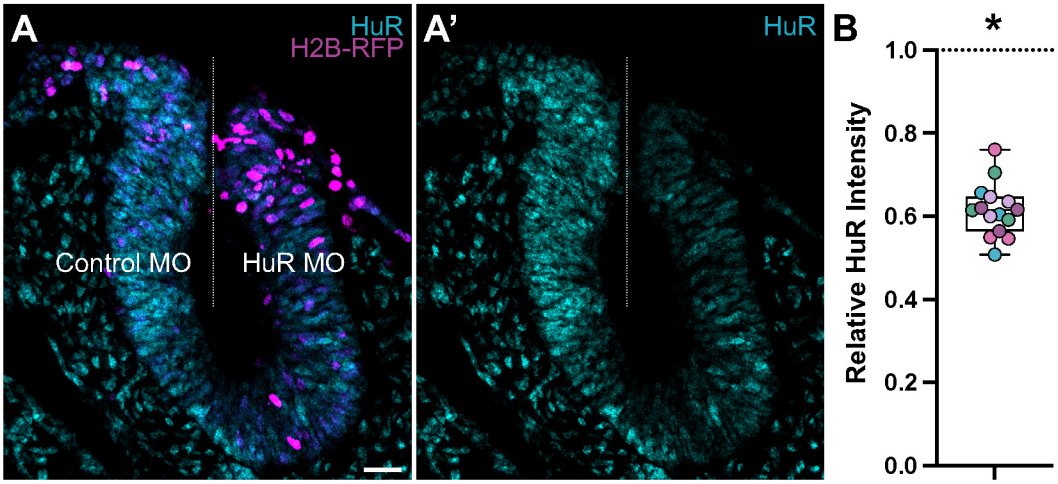

Figure 2—Supplement 1. Translation-blocking morpholino suppresses HuR expression.
(**A**) Representative confocal maximum intensity projection micrograph of cross-sectioned embryo bilaterally co-electroporated with a fluorescent electroporation control construct (H2B-RFP) and control morpholino (left) or HuR morpholino (right), immunostained for HuR (cyan). Dotted white line indicates midline. Scale bar, 20 μm.
(**B**) Relative fluorescence intensity of HuR for HuR knockdown compared to control sides of cross-sections, calculated as ratio of HuR morpholino versus control morpholino integrated density. Data are from individual sections; sections from same embryo are displayed in same color (n = 5 embryos, 15 sections) *, $P < 0.001$, paired *t*-test.

Figure 3—Supplement 1. Predicted HuR binding sites within the *Draxin* 3'-UTR.
A representative secondary structure of the *Draxin* 3'-UTR, predicted by 'mfold' analysis. Predicted HuR binding sites are highlighted in blue.

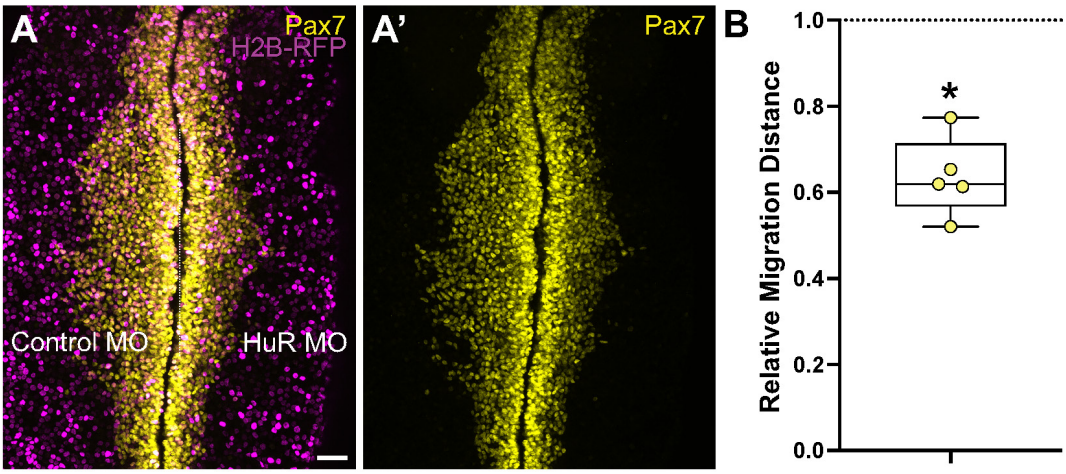

Figure 4—Supplement 1. HuR knockdown inhibits cranial neural crest EMT.
(**A**) Representative confocal maximum intensity projection micrograph of whole mount embryo bilaterally co-electroporated with a fluorescent electroporation control construct (H2B-RFP) and control morpholino (left) or HuR morpholino (right), immunostained for Pax7 (yellow). Dotted white line indicates midline. MO, morpholino. Scale bar, 50 µm.
(**B**) Relative migration distance for electroporated sides compared to control sides of whole mount embryos, calculated as ratio. Data are from individual embryos (n = 5 embryos, 5 measurements per embryo averaged). *, $P < 0.001$, paired *t*-test).